Research article

Gwang-Hun Jung[a], SeokJae Yoo[a] and Q-Han Park*

Measuring the optical permittivity of two-dimensional materials without *a priori* knowledge of electronic transitions

https://doi.org/10.1515/nanoph-2018-0120
Received August 12, 2018; revised September 14, 2018; accepted September 18, 2018

Abstract: We propose a deterministic method to measure the optical permittivity of two-dimensional (2D) materials without *a priori* knowledge of the electronic transitions over the spectral window of interest. Using the thin-film approximation, we show that the ratio of reflection coefficients for s and p polarization can give a unique solution to the permittivity of 2D materials within the measured spectral window. The uniqueness and completeness of our permittivity measurement method do not require *a priori* knowledge of the electronic transitions of a given material. We experimentally demonstrate that the permittivity of monolayers of MoS_2, WS_2, and WSe_2 in the visible frequency range can be accurately obtained by our method. We believe that our method can provide fast and reliable measurement of the optical permittivity of newly discovered 2D materials.

Keywords: two-dimensional materials; refractive index; ellipsometry; optical materials; characterization techniques.

1 Introduction

Atomically thin two-dimensional (2D) materials exhibit various distinct electronic and optical properties. At the early stage of 2D materials research, a single atomic layer of carbon, namely graphene, was intensively studied because this material is not only of fundamental importance to quantum electrodynamics but also has promising applications, such as in transparent electrodes [1], optical modulators [2], and infrared photodetectors [3]. In recent years, it was shown that the family of transition-metal dichalcogenides (TMDCs) can be obtained in atomically thin layers [4]. 2D TMDCs have a direct bandgap in the visible frequency region, while graphene does not. The energy bands in 2D TMDCs are also degenerate in the momentum space, namely valleys, and electrons can have the degree of freedom to populate each valley [5, 6]. The transitions at the bandgap in 2D TMDCs also give strong photoluminescence, and the polarization state of the emitted photons indicates which valleys give rise to the transitions [5, 6]. 2D TMDC-based optoelectronic devices have also been intensively studied because of the huge potential in valley-contrasting physics [7].

The permittivity of materials plays a pivotal role in the design of optoelectronic devices. For the family of 2D TMDCs, including MoS_2, $MoSe_2$, WS_2, and WSe_2, permittivity has been measured by ellipsometric spectroscopy [8–11]. To accurately obtain the permittivity of a given material using ellipsometric spectroscopy, we need *a priori* knowledge of their electronic transitions outside the spectral range of interest because conventional analysis methods for ellipsometric spectroscopy data fits the parameters of known spectral functions such as Lorentzian functions. For example, for permittivity measurements of 2D TMDCs in the visible frequency range, we have to know the location of their electronic transitions in the ultraviolet (UV) wavelength range because strong electronic transitions in the UV range can affect the permittivity in the visible range [9]. Therefore, we have to define the Lorentzian functions outside the spectral range of interest in the conventional measurement of the permittivity. To obtain the permittivity accurately without *a priori* knowledge on the electronic transitions, we have to measure the samples in the UV range, but this is often impossible because the high-energy UV light can damage the sample.

[a]**Gwang-Hun Jung and SeokJae Yoo:** These authors contributed equally to this work.
***Corresponding author: Q-Han Park,** Department of Physics, Korea University, Seoul 02841, Korea, e-mail: qpark@korea.ac.kr
Gwang-Hun Jung: Department of Physics, Korea University, Seoul 02841, Korea
SeokJae Yoo: Department of Physics, Korea University, Seoul 02841, Korea; and Department of Physics, University of California, Berkeley, CA 94720, USA. https://orcid.org/0000-0002-6438-7123

The field of 2D materials is emerging, and novel 2D materials are being discovered daily. Furthermore, the significant changes in their optoelectronic properties brought about by phase changes in their crystal structure [12], surface functionalization [13, 14], dielectric screening effects [15], external magnetic fields [16], and optical pumping [17] are being actively reported. However, despite these findings indicating that the properties of 2D materials are potentially highly tunable, in practice this tunability often makes it hard to measure their permittivity because of the lack of *a priori* knowledge of the electronic transitions of novel 2D materials over the wider spectral range including high-energy bands up to tens of electronvolts (eV).

In this paper, we propose a deterministic method for measuring the electric permittivity of 2D materials. In striking contrast to conventional measurement methods in ellipsometric spectroscopy, our method does not require *a priori* knowledge of the electronic transitions of materials outside the measured spectral window. Given the measured data, but without *a priori* knowledge of the 2D material, our measurement method yields unique and robust permittivity results, while the conventional methods based on parameter-fitting may predict permittivity with a large degree of error. We demonstrate that our method can provide accurate permittivity measurements for MoS_2, WS_2, and WSe_2 monolayers.

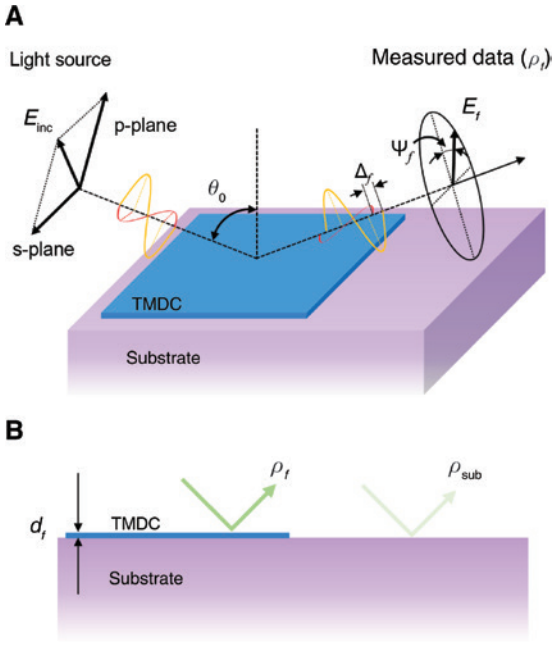

Figure 1: Principle of the deterministic permittivity measurement. (A) Schematic of the deterministic permittivity measurement of 2D materials. (B) Complex reflection ratio of the 2D thin film material of thickness d_f on the substrate (ρ_f) and of the bare substrate (ρ_{sub}). E_f is the reflected field when the incident field E_{inc} impinges on the sample with the angle of incidence θ_0. Reflectivity can be characterized by the reflection amplitude ratio tan(ψ) and the phase difference Δ.

2 Results

2.1 Deterministic measurement of the refractive index

We suggest a method to directly measure the refractive index of 2D materials using conventional spectroscopic ellipsometers. These conventional instruments measure the complex ratio of the reflection coefficients for p- and s-polarized light, i.e. $\rho = r^{(p)}/r^{(s)}$, within a finite spectral range. Figure 1 shows a schematic of the measurement procedures. Suppose that a thin film of 2D material of thickness d_f and refractive index n_f is prepared on a dielectric substrate of refractive index n_{sub}. The light beam impinges on the thin film from the upper half-plane with the index n_0. We measure the complex reflection ratio of both the thin 2D film material on the substrate (ρ_f) and the bare substrate alone (ρ_{sub}). Since the thin 2D film material is atomically thin, we can approximate the complex reflection ratio by

$$\begin{aligned}\rho_f(\phi) &= \rho_f\big|_{\phi=0} + \left.\frac{\mathrm{d}\rho_f}{\mathrm{d}\phi}\right|_{\phi=0}\phi \\ &= \rho_{\mathrm{sub}}\left\{1+\left(\frac{1}{r_f^{(p)}}\frac{\mathrm{d}r_f^{(p)}}{\mathrm{d}\phi}-\frac{1}{r_f^{(s)}}\frac{\mathrm{d}r_f^{(s)}}{\mathrm{d}\phi}\right)\right|_{\phi=0}\phi\Bigg\},\end{aligned} \tag{1}$$

using the Taylor expansion for the optical path length $\phi = n_f k_0 d_f \cos\theta_f$ in the 2D thin film material, with the vacuum wavenumber $k_0 = 2\pi/\lambda$, the wavelength of light λ, the propagating angle of light inside the 2D material θ_F, and the reflection coefficients of the thin 2D film material on the substrate for p-polarized (s-polarized) light $r_f^{(p)}$ ($r_f^{(s)}$). The angle θ_F is determined by Snell's law, $n_F \sin\theta_F = n_0 \sin\theta_0$, with the incidence angle of light θ_0. Note that we used the relation $\rho_{\mathrm{subs}} = (r_f^{(p)}/r_f^{(s)})\big|_{\phi=0}$ to derive Eq. (1). The reflection coefficients $r_f^{(p,s)}$ are given by

$$r_f^{(p,s)} = \frac{r^{(p,s)}(n_0, n_f, \theta_0)\mathrm{e}^{-i\phi} + r^{(p,s)}(n_f, n_{\mathrm{sub}}, \theta_f)\mathrm{e}^{i\phi}}{\mathrm{e}^{-i\phi} + r^{(p,s)}(n_0, n_f, \theta_0)r^{(p,s)}(n_f, n_{\mathrm{sub}}, \theta_f)\mathrm{e}^{i\phi}}, \tag{2}$$

Then, the terms in the round bracket in Eq. (1) evaluated at $\phi = 0$ can be written as

$$\frac{1}{r_f^{(p,s)}}\frac{\mathrm{d}r_f^{(p,s)}}{\mathrm{d}\phi}\bigg|_{\phi=0} = 2i\frac{\left\{r^{(p,s)}(n_0, n_{\mathrm{sub}}, \theta_0) - r^{(p,s)}(n_0, n_f, \theta_0)\right\}\left\{1 - r^{(p,s)}(n_0, n_{\mathrm{sub}}, \theta_0)r^{(p,s)}(n_0, n_f, \theta_0)\right\}}{r^{(p,s)}(n_0, n_{\mathrm{sub}}, \theta_0)\left\{1 - r^{(p,s)}(n_0, n_f, \theta_0)^2\right\}}, \tag{3}$$

where the reflection coefficients at the interface of the two media with the refractive indices n_0 and n are given by

$$r^{(p)}(n_0, n, \theta_0) = \frac{n_0\sqrt{n^2 - n_0^2\sin^2\theta_0} - n^2\cos\theta_0}{n_0\sqrt{n^2 - n_0^2\sin^2\theta_0} + n^2\cos\theta_0}, \tag{4}$$

$$r^{(s)}(n_0, n, \theta_0) = \frac{n_0\cos\theta_0 - \sqrt{n^2 - n_0^2\sin^2\theta_0}}{n_0\cos\theta_0 + \sqrt{n^2 - n_0^2\sin^2\theta_0}}. \tag{5}$$

Plugging Eqs. (3–5) into Eq. (1), we can obtain the quadratic equations for the refractive index of the 2D thin film material as

$$\left(n_f^2 - n_{\mathrm{sub}}^2\right) + \varepsilon_{\mathrm{inc}}\left(\frac{n_{\mathrm{sub}}^2}{n_f^2} - 1\right) = \frac{1}{\alpha}\left(\frac{\rho_f}{\rho_{\mathrm{sub}}} - 1\right), \tag{6}$$

where the function α is given by

$$\alpha = 4ik_0 d_f \frac{n_0 n_{\mathrm{sub}}^2\cos(\theta_0)\sin^2(\theta_0)}{\left(n_0^2 - n_{\mathrm{sub}}^2\right)\left\{n_{\mathrm{sub}}^2 - n_0^2 + \left(n_{\mathrm{sub}}^2 + n_0^2\right)\cos(2\theta_0)\right\}}. \tag{7}$$

The solution of Eq. (6) can be expressed in the form

$$n_f^2 = \frac{1}{2}\left\{n_0^2 + n_{\mathrm{sub}}^2 + (\delta_\rho/\alpha)\right\} \pm \frac{1}{2}\sqrt{\left\{n_0^2 + n_{\mathrm{sub}}^2 + (\delta_\rho/\alpha)\right\}^2 - 4n_0^2 n_{\mathrm{sub}}^2}, \tag{8}$$

where $\delta_\rho = (\rho_f - \rho_{\mathrm{sub}})/\rho_{\mathrm{sub}}$ is the fractional change in the complex reflection ratio.

The ambiguity of the sign in Eq. (8) can be resolved by imposing the passivity condition $\mathrm{Im}(n_f) > 0$. The expression for the refractive index of 2D materials, Eq. (8), is the key result of this paper. We can directly obtain the refractive index n_f from the measured quantities ρ_f and ρ_{sub}. It requires neither the fitting procedures for the spectral line shape functions nor *a priori* knowledge of the electronic transitions of the 2D materials. Using our method, the deterministic solution for the permittivity can be obtained from the given measurement data.

2.2 Refractive indices of monolayer TMDCs

We apply our method to monolayer TMDCs, which are promising 2D materials possessing semiconductor properties, with their direct bandgap in visible wavelengths and their spin-valley properties [5, 18]. Large-area, uniform films of monolayer MoS_2, WS_2, and WSe_2 were purchased from SixCarbon and prepared on sapphire (Al_2O_3) wafers. We measured their complex reflection ratios and the permittivity of the sapphire substrate using a commercial spectroscopic ellipsometer (alpha-SE, JA Woollam), which is used throughout this paper.

Figure 2A–C shows the Raman spectra of MoS_2, WS_2, and WSe_2 monolayers. In Figure 2A, the MoS_2 monolayer presents two sharp peaks at 385.48 (E^1_{2g}) and 402.90 cm^{-1} (A_{1g}), which correspond to the first-order in-plane and out-of-plane modes at the Brillouin zone center, respectively [19]. The frequency difference between the E^1_{2g} and A_{1g} modes is $\Delta\omega = 17.42$ cm^{-1}, which is indicative of the MoS_2 monolayer [6]. In Figure 2B, the WS_2 monolayer presents a peak at 348.93 cm^{-1} (A_{1g}) with a shoulder at 330.32 cm^{-1} (2LA). The shoulder originates from the second-order longitudinal acoustic (LA) phonon mode, and is indicative of the WS_2 monolayer [20]. In Figure 2C, the WSe_2 monolayer presents a peak emerging at 250.53 cm^{-1} due to the first-order out-of-plane mode (A_{1g}). It is known that this strikingly sharp peak disappears when the WSe_2 layer increases in thickness to a few layers more than a bilayer [19] and that the emergence of the sharp A_{1g} peak is indicative of a WSe_2 monolayer.

We also use the optical contrast of the monolayers on the Si/SiO_2 wafer to confirm that the TMDC monolayers are really monolayers. The optical contrast is defined as $(I - I_{\mathrm{sub}})/I_{\mathrm{sub}}$ using the image intensities I (I_{sub}) of the 2D TMDCs (the bare substrate). The interference of light from the SiO_2 spacer layer on the Si substrate allows the number of layers of 2D TMDCs to be confirmed by optical contrast [21]. When the optical contrast of the 2D TMDC flakes lies between 0.25 and 0.4, we can conclude that they are composed of a monolayer [21]. First, the samples of monolayers MoS_2, WS_2, and WSe_2 were transferred to Si/SiO_2 wafers with an oxide thickness of 280 nm, and optical images were then recorded using a charge-coupled device (CCD) camera. Figure 2D–F shows the optical contrast of the monolayers of MoS_2, WS_2, and WSe_2 along with the black lines of the optical images in the insets. The optical contrasts of our samples lie between 0.25 and 0.4, indicating that they are monolayers [21].

Figure 3 shows the permittivity spectra of monolayers of MoS_2, WS_2, and WSe_2 in the visible spectral

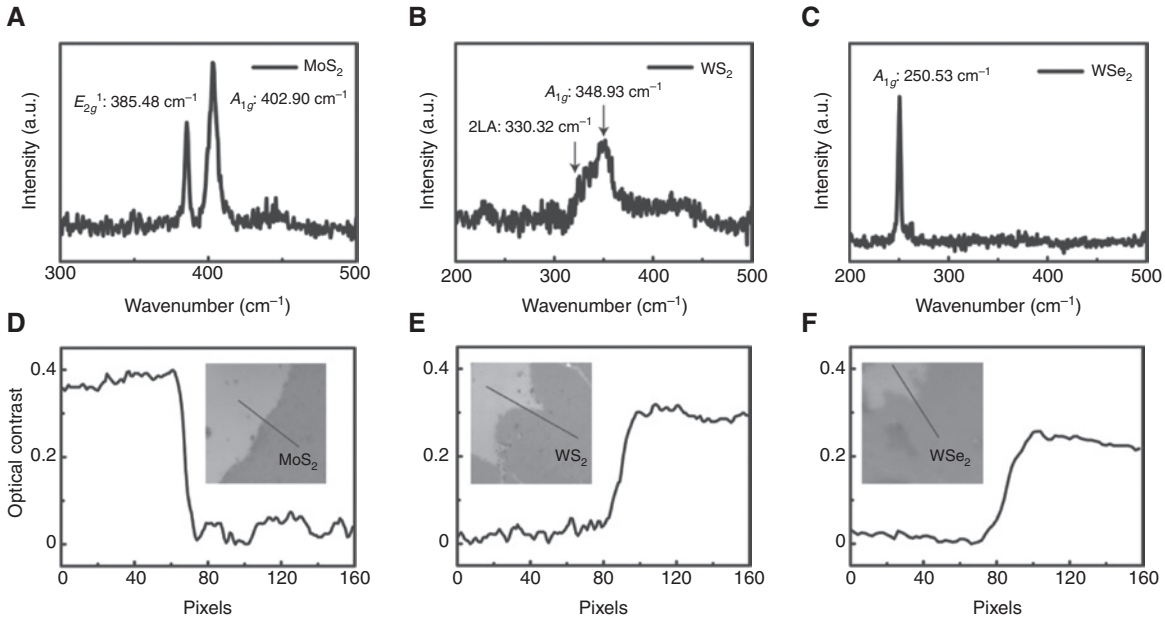

Figure 2: Confirmation of monolayer TMDCs.
Raman spectra of monolayers of (A) MoS_2, (B) WS_2, and (C) WSe_2. The optical contrast of monolayer (D) MoS_2, (E) WS_2, and (F) WSe_2 along the black lines in the optical images in the insets.

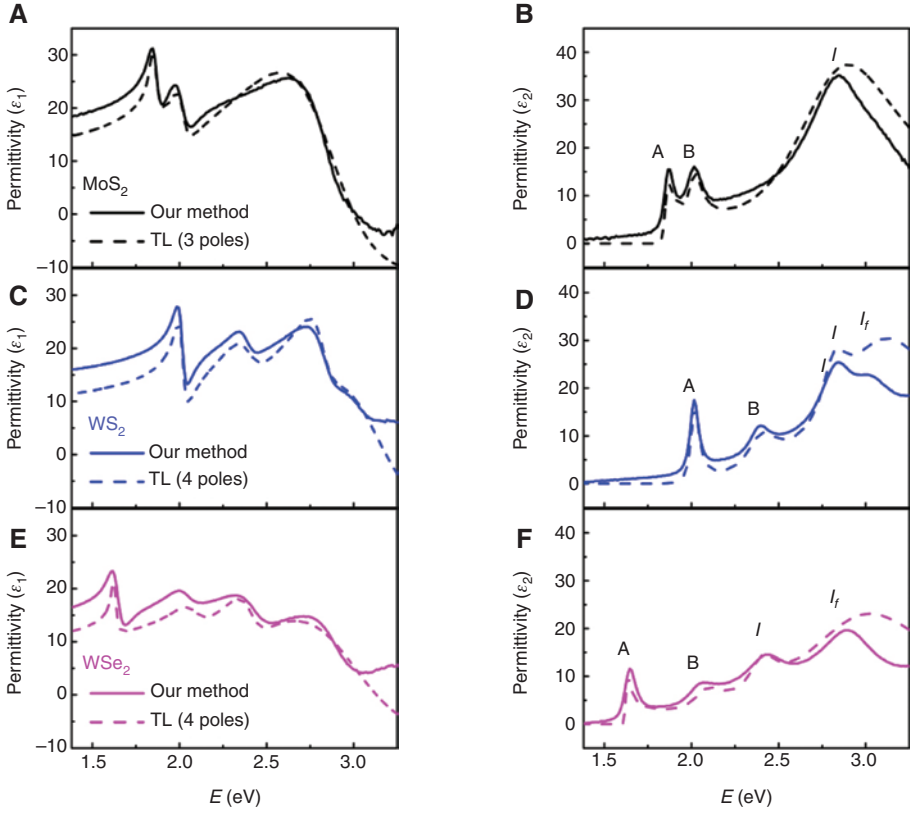

Figure 3: The permittivity of monolayer TMDCs.
Real (left column) and the imaginary part (right column) of the permittivity of monolayers of (A, B) MoS_2, (C, D) WS_2, and (E, F) WSe_2. Solid and dashed lines, respectively, correspond to the data obtained by our method and by Tauc–Lorentz fitting with a limited number of poles (see Supporting Information for the tabulated data of the permittivity and the refractive index plotted in Figure 3).

range, obtained using Eq. (8). For all monolayers TMDCs, the A and B exciton bands can be found using the peaks of the imaginary part of the measured permittivity near the energy of 2.0 eV. At the higher energy band near 3.0 eV, the strong interband transition (peak *I*) and its fine structure (peak I_f) are observed [8]. For monolayers WS_2 and WSe_2 (Figure 3B,C), their interband transitions and fine structure are clearly resolved, while for monolayer MoS_2 the fine structure is barely visible (Figure 2A). By resolving these peaks, we demonstrate that the permittivity of 2D TMDCs can be obtained without *a priori* knowledge of the electronic transitions in the visible frequency range. In the next section, we will confirm that our method is not influenced by knowledge of the strong electronic transitions outside the spectral window.

2.3 Effect of *a priori* knowledge of high-energy electronic transitions on permittivity measurements

Conventional spectroscopic ellipsometry methods for semiconductor materials use Tauc–Lorentzian (TL) spectral line shape functions to describe the permittivity of these materials [9, 22]. The imaginary permittivity can be written as the sum of the *N* TL functions, i.e. $\mathrm{Im}\,\varepsilon(E)=\sum_{k=1}^{N}\mathrm{Im}\,\varepsilon_k(E)$ with

$$\begin{aligned}\mathrm{Im}\,\varepsilon_k(E)&=\frac{A_k(E_0)_k C_k(E-E_b)^2}{(E^2-E_{0,k}^2)^2+C_k{}^2E^2}\frac{1}{E}\ \text{ for }\ E>E_{b,k},\\&=0\ \text{ for }\ E\le E_{b,k},\end{aligned}\tag{9}$$

with the amplitude *A*, the broadening *C*, the photon energy *E*, the peak transition energy E_0, and the bandgap E_b. The subscript *k* in Eq. (9) denotes the parameters of the *k*th pole. Each TL function corresponds to the respective electric transitions of the material. The real part of the permittivity can be obtained by the Kramers–Kronig relation [23]

$$\mathrm{Re}\,\varepsilon(E)=1+\frac{2}{\pi}P\int_{E_b}^{\infty}\frac{\xi\,\mathrm{Im}\,\varepsilon(\xi)}{\xi^2-E^2}\mathrm{d}\xi.\tag{10}$$

Equation (9) automatically gives the constraints to the obtained permittivity satisfying the Kramers–Kronig relation, resulting in a causal description of the optical response of the materials. However, this approach requires *a priori* knowledge of the materials because electronic transitions outside the spectral range of interest can affect the analysis of the permittivity in the finite spectral range. For example, high-energy electronic transitions up to 30 eV should be taken into account for the permittivity of monolayer TMDCs within the narrow visible spectral range of 1.5–3.0 eV [9]. Higher energy electronic transitions are generally very strong, and their off-resonant tails can reach the visible spectral range. If these high-energy electronic transitions are neglected in the analysis of the permittivity, it may lead to multiple results satisfying the same reflectivity spectrum.

In Figure 4, we demonstrate how, when using the *N* TL spectral functions, high-energy electronic transitions outside the spectral range of interest influence the permittivity analysis, i.e. Eq. (9). We numerically find the TL parameters in Eq. (9) that fit the experimentally measured spectra of the reflection ratio, i.e. $\rho=r^{(p)}/r^{(s)}=\tan(\Psi)e^{i\Delta}$, with the reflection amplitude ratio $\tan(\psi)$ and the phase difference Δ. The accuracy of the spectral fitting is determined for a given number of TL functions *N*. In contrast, our deterministic index analysis method, based on Eq. (8), does not depend on *N*. In Figure 4, we compare the errors made by these two permittivity analysis methods. The error can be evaluated by $\delta\psi=\psi_{exp}-\psi_{mod}$ and $\delta\Delta=\Delta_{exp}-\Delta_{mod}$, where ψ_{exp} and ψ_{mod} (Δ_{exp} and Δ_{mod}) are the reflection amplitude ratio ψ (the phase difference Δ) of the experimental results and the model results, respectively. Without *a priori* knowledge of the electronic transitions in the material, the function number *N* is determined by the number of peaks in the visible frequency range, i.e. $N_{vis}=3$ ($N_{vis}=4$) for monolayer MoS_2 (WS_2 and WSe_2). As shown in Figure 4, TL function analysis using the function number $N=N_{vis}$ does not provide a perfect fit for the experimentally measured ψ_{exp} and Δ_{exp}. Note that the error made by the TL function analysis is significant even for the A and B exciton bands, which are far from the higher energy bands with interband transitions. This implies that the optical response of monolayer TMDCs across the entire visible frequency range is also influenced by higher energy electronic transitions such as the fine structures of the interband transition, partial plasma resonances, and the full plasma excitation involving all valence electrons [8]. On the other hand, our deterministic analysis method shows reduced error compared to the TL function analysis with the function number $N=N_{vis}$. We also note that the errors $\delta\psi$ and $\delta\Delta$ in our method tend to increase in the high-energy bands near 3.0 eV because the thin-film approximation starts to fail, but this does not significantly affect the visible frequency range in which the A and B exciton bands are located. Table 1 summarizes the spectral average of the errors given by $\langle\delta\Psi\rangle=\left\{\int_{\omega_1}^{\omega_2}\delta\Psi(\omega)d\omega\right\}\Big/(\omega_2-\omega_1)$ and $\langle\delta\Delta\rangle=\left\{\int_{\omega_1}^{\omega_2}\delta\Delta(\omega)d\omega\right\}\Big/(\omega_2-\omega_1)$ for the two methods.

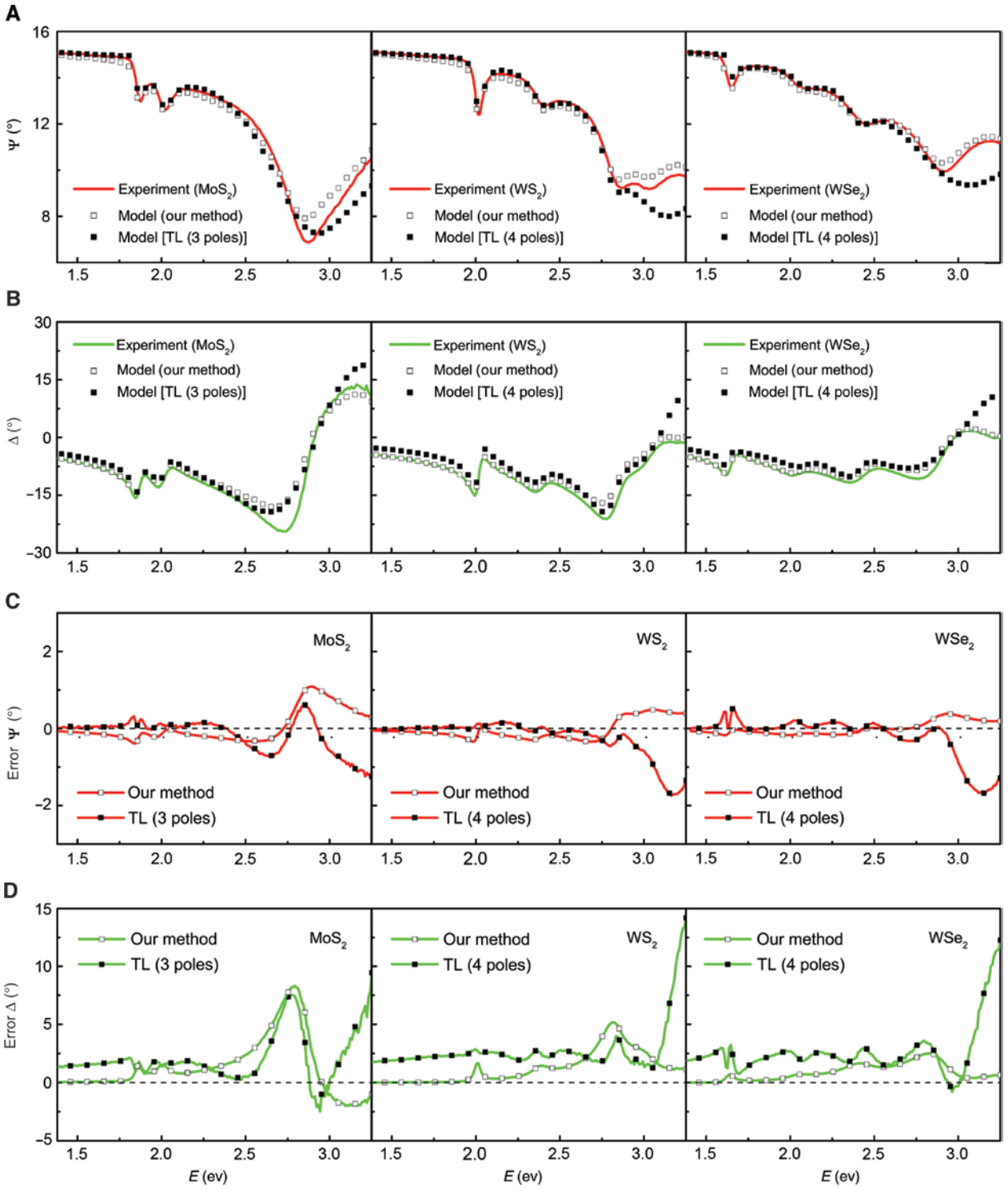

Figure 4: The errors compared to the conventional method.
(A) Reflection amplitude ratio (ψ) and (B) phase difference Δ. Solid lines: experimental results; white squares: results of our method; black squares: results of TL fitting with *N* poles. (C) Errors in the amplitude ratio ⟨δψ⟩ and (D) errors in the phase difference ⟨δΔ⟩ of monolayers of MoS_2 (left column), WS_2 (middle column), and WSe_2 (right column). Solid lines with white squares show the errors in the results of our method and solid lines with black squares are the errors in the results of the TL fitting method with *N* poles.

Table 1: Summary of the spectral averaged errors $\langle\delta\psi\rangle$ and $\langle\delta\Delta\rangle$.

Materials	Our deterministic analysis		Tauc–Lorentzian analysis	
	$\langle\delta\psi\rangle$	$\langle\delta\Delta\rangle$	$\langle\delta\psi\rangle$	$\langle\delta\Delta\rangle$
Monolayer MoS_2	0.32	1.88	0.30	2.22
Monolayer WS_2	0.23	1.27	0.27	2.77
Monolayer WSe_2	0.13	0.88	0.31	2.63

It shows that the spectral averages of the errors of our analysis method are smaller than those of the TL analysis method.

2.4 Effect of anisotropy of the 2D materials

It is also worth noting that the permittivity of the 2D materials can be described in the tensor form

$$\boldsymbol{\varepsilon} = \begin{pmatrix} \varepsilon_{\parallel} & 0 & 0 \\ 0 & \varepsilon_{\parallel} & 0 \\ 0 & 0 & \varepsilon_{\perp} \end{pmatrix} \tag{11}$$

with the in-plane permittivity $\varepsilon_{\parallel}$ and the out-of-plane permittivity $\varepsilon_{\perp}$ because of material anisotropy. Using the anisotropic permittivity tensor, we can relate the in-plane and out-of-plane permittivities with the complex reflection ratio. In the same manner as when deriving Eq. (6), the relation is given by

$$\left(\varepsilon_{\parallel} - n_{\text{sub}}^2\right) + \varepsilon_{\text{inc}}\left(\frac{n_{\text{sub}}^2}{\varepsilon_{\perp}} - 1\right) = \frac{1}{\alpha}\left(\frac{\rho_f}{\rho_{\text{sub}}} - 1\right). \tag{12}$$

Equation (12) shows that the in-plane permittivity $\varepsilon_{\parallel}$ and the out-of-plane permittivity $\varepsilon_{\perp}$ cannot be simultaneously determined by our method. However, we can find that the effect of the out-of-plane permittivity $\varepsilon_{\perp}$ becomes significant when $\varepsilon_{\perp}$ is small. The zero out-of-plane permittivity, i.e. $\varepsilon_{\perp} = 0$, falls into the singularity of the term $n_{\text{sub}}^2/\varepsilon_{\perp}$ in Eq. (12), but only for metallic materials whose permittivity decreases to the point of becoming negative. However, for most 2D materials, the out-of-plane permittivity is unlikely to become metallic [24]. Therefore, we can speculate that the anisotropic effect on permittivity is insignificant for the optical response of 2D materials.

3 Conclusion

Although our method allows the determination of the permittivity of 2D materials without *a priori* knowledge, it can result in significant errors in two specific cases: (1) in high-frequency regions and (2) for large refractive index of 2D materials, because cases of both high frequencies $\omega = ck_0$ and large refractive indices n_f increase the optical path length $\phi = n_f k_0 d$. In our method, a large optical path length ϕ results in the breakdown of the first-order approximation of the optical path length ϕ [Eq. (1)]. Therefore, we would like to emphasize that for these two cases careful consideration is required.

To sum up, we have provided a method to measure and analyze the permittivity of 2D materials. We showed that the first-order approximation of the optical path length ϕ for the complex reflection ratio ρ in ellipsometric spectroscopy measurements can provide the deterministic permittivity of 2D materials without *a priori* knowledge of the 2D material or parameter-fitting for a certain spectral function. Using monolayer MoS_2, WS_2, and WSe_2 as test cases, we showed that our method can provide robust permittivity measurements. We expect that our method can provide a fast, robust, and accurate way to determine the optical properties of newly discovered 2D materials.

Acknowledgments: This work was supported by the Samsung Science and Technology Foundation under Project No. SSTF-BA1401-05. SeokJae Yoo was supported by the Basic Science Research Program through the National Research Foundation of Korea (NRF) funded by the Ministry of Education (2017R1A6A3A11034238).

References

[1] Wang X, Zhi L, Müllen K. Transparent, conductive graphene electrodes for dye-sensitized solar cells. Nano Lett 2008;8:323–7.
[2] Liu M, Yin X, Ulin-Avila E, et al. A graphene-based broadband optical modulator. Nature 2011;474:64–7.
[3] Yu T, Wang F, Xu T, Ma L, Pi X, Yang D. Graphene coupled with silicon quantum dots for high-performance bulk-silicon-based schottky-junction photodetectors. Adv Mater 2016;28:4912–9.
[4] Splendiani A, Sun L, Zhang Y, et al. Emerging photoluminescence in monolayer MoS_2. Nano Lett 2010;10:1271–5.
[5] Mak KF, He K, Shan J, Heinz TF. Control of valley polarization in monolayer MoS_2 by optical helicity. Nat Nanotechnol 2012;7:494–8.
[6] Zeng H, Dai J, Yao W, Xiao D, Cui X. Valley polarization in MoS2 monolayers by optical pumping. Nat Nanotechnol 2012;7:490–3.
[7] Schaibley JR, Yu H, Clark G, et al. Valleytronics in 2D materials. Nat Rev Mater 2016;1:16055.
[8] Beal AR, Hughes HP. Kramers-Kronig analysis of the reflectivity spectra of 2H-MoS_2, 2H-$MoSe_2$ and 2H-$MoTe_2$. J Phys C Solid State Phys 1979;12:881–90.

[9] Li Y, Chernikov A, Zhang X, et al. Measurement of the optical dielectric function of monolayer transition-metal dichalcogenides: MoS_2, $MoSe_2$, WS_2 and WSe_2. Phys Rev B 2014;90:1–6.
[10] Zhang H, Ma Y, Wan Y, et al. Measuring the refractive index of highly crystalline monolayer MoS_2 with high confidence. Sci Rep 2015;5:1–7.
[11] Liu HL, Shen CC, Su SH, et al. Optical properties of monolayer transition metal dichalcogenides probed by spectroscopic ellipsometry. Appl Phys Lett 2014;105:201905.
[12] Kang Y, Najmaei S, Liu Z, et al. Plasmonic hot electron induced structural phase transition in a MoS_2 monolayer. Adv Mater 2014;26:6467–71.
[13] Chen X, McDonald AR. Functionalization of two-dimensional transition-metal dichalcogenides. Adv Mater 2016;28:5738–46.
[14] Nguyen EP, Carey BJ, Ou JZ, et al. Electronic tuning of 2D MoS_2 through surface functionalization. Adv Mater 2015;27: 6225–9.
[15] Hüser F, Olsen T, Thygesen KS. How dielectric screening in two-dimensional crystals affects the convergence of excited-state calculations: monolayer MoS_2. Phys Rev B 2013;88:245–309.
[16] Srivastava A, Sidler M, Allain AV, Lembke DS, Kis A, Imamoglu A. Valley Zeeman effect in elementary optical excitations of monolayer WSe_2. Nat Phys 2015;11:141–7.
[17] Kim J, Jin C, Chen B, et al. Observation of ultralong valley lifetime in WSe_2/MoS_2 heterostructures. Sci Adv 2017;3:e1700518.
[18] Xiao D, Bin Liu G, Feng W, Xu X, Yao W. Coupled spin and valley physics in monolayers of MoS_2 and other group-VI dichalcogenides. Phys Rev Lett 2012;108:1–5.
[19] Tonndorf P, Schmidt R, Böttger P, et al. Photoluminescence emission and Raman response of monolayer MoS_2, $MoSe_2$, and WSe_2. Opt Exp 2013;21:4908.
[20] Berkdemir A, Gutiérrez HR, Botello-Méndez AR, et al. Identification of individual and few layers of WS_2 using Raman spectroscopy. Sci Rep 2013;3:1755.
[21] Benameur MM, Radisavljevic B, Héron JS, Sahoo S, Berger H, Kis A. Visibility of dichalcogenide nanolayers. Nanotechnology 2011;22:125706.
[22] Liu HL, Shen CC, Su SH, Hsu CL, Li MY, Li LJ. Investigation of the optical properties of MoS_2 thin films using spectroscopic ellipsometry. Appl Phys Lett 2014;104:103114.
[23] Jackson JD. Classical electrodynamics. Weinheim, Germany: Wiley-VCH Verlag GmbH & Co. KGaA, 1998.
[24] Laturia A, Van de Put ML, Vandenberghe WG. Dielectric properties of hexagonal boron nitride and transition metal dichalcogenides: from monolayer to bulk. NPJ 2D Mater Appl 2018;2:6.

Supplementary Material: The online version of this article offers supplementary material (https://doi.org/10.1515/nanoph-2018-0120).